Structural Characterization and Thermal Stability of MoS_2 Intercalation Compounds

Keenan E. Dungey, M. David Curtis,* and James E. Penner-Hahn

Willard H. Dow Laboratory, Department of Chemistry, The University of Michigan, Ann Arbor, Michigan 48109-1055

Received January 21, 1998. Revised Manuscript Received May 18, 1998

The intercalation of MoS_2 with Co and Fe complexes has been accomplished via exfoliation of Li_xMoS_2 by reaction with water, followed by flocculation in the presence of cationic guest species. The resulting self-assembled compounds have been characterized by X-ray absorption spectroscopy, electron diffraction, powder X-ray diffraction, and magnetic measurements. The 2H-type (undistorted) MoS_2 undergoes a structural distortion to 1T-type MoS_2 during the Li intercalation, which is partially maintained upon exfoliation and flocculation. A structural model of 1T-MoS_2 is proposed on the basis of X-ray absorption spectroscopy and electron diffraction, in which the unit cell has *P*3 symmetry with lattice parameters $a = 6.52(5)$ Å, $c = 6.14$ Å. The Mo atoms are shifted approximately 0.5 Å from their positions in 2H-MoS_2 to form trigonal clusters in 1T-MoS_2, with a concomitant change in coordination geometry from trigonal prismatic to distorted octahedral. Layers of Co-$(OH)_2$ were intercalated between the distorted and/or undistorted layers of MoS_2 when either Co^{2+} or Co^{3+} complexes were used as the flocculating ion. Flocculation of exfoliated MoS_2 with $(\eta^5\text{-}C_5H_5)_2M^+$ (M = Fe, Co) resulted in intercalation of monolayers of the metallocenium cations between the partially negatively charged MoS_2 sheets.

Introduction

The engineering of structures on a nanoscale is an intense area of research for the production of new materials with optical, conductive, and catalytic applications.[1] One approach to modify the properties of a material has been through the intercalation of guests into a host, such as clays and graphite.[2,3] Many transition metal dichalcogenides have lamellar structures amenable to intercalation, and such modified materials could have interesting applications. In particular, MoS_2 has applications as a catalyst for hydrodesulfurization (HDS), and the intercalation of promoter elements (Co, Ni) may result in improved catalytic activity. However, intercalation of MoS_2 has only been possible with small, strongly reducing guests (e.g. the alkali metals).[4] Cp_2Co ($Cp = \eta^5\text{-}C_5H_5$), although a good reducing agent, proved to be too large for direct intercalation.[5] A route to intercalated MoS_2 has been developed that entails initial intercalation with Li, followed by aqueous exfoliation, and subsequent restacking of the suspension of single layer MoS_2 around the guest.[6]

The exfoliation technique has been used to modify MoS_2 for many materials applications, including as an inorganic host for conducting polymers,[7−10] an encapsulating support for magnetic materials,[11,12] a catalyst support,[13−15] and a coal liquefaction catalyst.[16] Recently this technique was used to form pillared materials by intercalation with cobalt sulfide clusters.[17] The compounds of MoS_2 intercalated with Co species described here have been used as HDS catalyst precursors.[18]

Multiple studies have been aimed at elucidating the structure of single-layer MoS_2 produced by the exfoliation technique. Formation of a $2 \times 2a_o$ superlattice has been observed in the Li-intercalated MoS_2[19] and was also recently reported for exfoliated and restacked

(1) For a recent summary of nanostructured materials, see the August 1996 issue of *Chem. Mater.* [*Chem. Mater.* **1996**, *8* (8)].
(2) *Progress in Intercalation Research*; Müller-Warmuth, W., Schöllhorn, R., Eds.; Kluwer: London, 1994.
(3) *Chemical Physics of Intercalation II*; Bernier, P., Fischer, J. E., Roth, S., Solin, S. A., Eds.; Plenum: New York, 1993.
(4) Thompson, A. H.; Di Salvo, F. J. In *Intercalation Chemistry*; Whittingham, M. S., Jacobson, A. J., Eds.; Academic: New York, 1982; p 573.
(5) Blekkan, E. A.; Mitchell, P. V. *Bull. Soc. Chim. Belg.* **1987**, *96*, 961.
(6) Gee, M. A.; Frindt, R. F.; Joensen, P.; Morrison, S. R. *Mater. Res. Bul.* **1986**, *21*, 543.
(7) Divigalpitiya, W. M. R.; Frindt, R. F.; Morrison, S. R. *J. Mater. Res.* **1991**, *6*, 1103.
(8) Ruiz-Hitzky, E.; Jimenez, R.; Casal, B.; Manriquez, V.; Santa Ana, A.; Gonzalez, G. *Adv. Mater.* **1993**, *5*, 738.
(9) Bissessur, R.; Kanatzidis, M. G.; Schindler, J. L.; Kannewurf, C. R. *J. Chem. Soc., Chem. Commun.* **1993**, 1582.
(10) Wang, L.; Schindler, J.; Thomas, J. A.; Kannewurf, C. R.; Kanatzidis, M. G. *Chem. Mater.* **1995**, *7*, 1753.
(11) Frindt, R. F.; Arrott, A. S.; Curzon, A. E.; Heinrich, B.; Morrison, S. R.; Templeton, T. L.; Divigalpitiya, R.; Gee, M. A.; Joensen, P.; Schurer, P. J.; LaCombe, J. L. *J. Appl. Phys.* **1991**, *70*, 6224.
(12) Templeton, T. L.; Yoshida, Y.; Li, X.-Z.; Arrott, A. S.; Curzon, A. E.; Hamed, F.; Gee, M. A.; Schurer, P. J.; LaCombe, J. L. *IEEE Trans. Magn.* **1993**, *29*, 2625.
(13) Miremadi, B. K.; Morrison, S. R. *J. Catal.* **1987**, *103*, 334.
(14) Miremadi, B. K.; Morrison, S. R. *J. Catal.* **1988**, *112*, 418.
(15) Scholz, G. A.; Morrison, S. R. *Can. J. Chem.* **1989**, *67*, 862.
(16) Bockrath, B. C.; Parfitt, D. S. *Catal. Lett.* **1995**, *33*, 201.
(17) Bissessur, R.; Heising, J.; Hirpo, W.; Kanatzidis, M. *Chem. Mater.* **1996**, *8*, 318.
(18) Dungey, K. E.; Curtis, M. D.; Penner-Hahn, J. E. *J. Catal.* **1998**, *175*, 129−134.
(19) Chrissafis, K.; Zamani, M.; Kambas, K.; Stoelmenos, J.; Economou, N. A.; Samaras, I.; Julien, C. *Mater. Sci. Eng. B* **1989**, *3*, 145.

S0897-4756(98)00034-9 CCC: $15.00
Published on Web 07/11/1998

WS_2.[20] A distorted structure was likewise implied by the detection of short and long Mo−Mo distances in the EXAFS of aqueous suspensions of single-layer MoS_2.[21] Powder X-ray diffraction[22] and Raman[23] studies indicate that the Mo is octahedrally coordinated in these distorted structures. Detailed Raman spectroscopy indicated that the octahedral coordination was distorted and that there was a $2 \times 1a_o$ superlattice,[24] which was confirmed by STM images of single layer MoS_2 on graphite.[25,26] However, AFM images of single layers of MoS_2 on mica indicated no superlattice formation.[27] Combined STM and AFM studies of ReS_2 demonstrated that these techniques image the top layer of sulfur atoms, and the images depend greatly upon the surface density of states (DOS).[28] On the other hand, Schöllhorn has reported the oxidation of K_xMoS_2 to synthesize 1T-type (distorted) MoS_2, which has a $\sqrt{3}a_o$ superlattice by powder X-ray diffraction.[29] A recent AFM study of $K_x(H_2O)_yMoS_2$ also exhibited a $\sqrt{3}a_o$ superlattice.[30] Neutron diffraction experiments are in progress to elucidate the atomic positions in 1T-MoS_2.[31]

As the exfoliation technique produces powdered materials, single crystal X-ray diffraction studies have not been possible. Therefore, multiple techniques have necessarily been utilized to obtain structural information. However, the literature up to this point presents conflicting models for the structure of single-layer MoS_2. Herein is proposed a structural model of exfoliated and restacked MoS_2, based upon combined electron diffraction, powder X-ray diffraction, and X-ray absorption structural characterization techniques. Cobalt and iron intercalation compounds of MoS_2 are characterized, and the first EXAFS study of Li_xMoS_2 is reported. In addition, the thermal stability of these materials is explored.

Experimental Section

General. $[Cp_2Co]PF_6$,[32] Cp_2Co,[33] $[Co(NH_3)_6]Cl_3$,[34] and Li_x-MoS_2 (**1**)[35] ($x = 0.85$, 3.55 wt % Li) were prepared by standard literature procedures. Other chemicals were purchased from Aldrich Chemical Co. or Strem Chemicals Inc. and used as received.

Centrifugation was performed on a Clay-Adams Safeguard Centrifuge. Ultracentrifugation at 0° C was done on a Sorvall Superspeed RC2−B, while a RC5−B was used for room-temperature centrifugation. Both used a SS-34 or GSA rotor, with 50 mL poly(propylene) round centrifuge tubes with push caps or 250 mL poly(propylene) centrifuge bottles with screw caps, respectively. UV−vis absorption spectra were taken on an Shimadzu UV160U spectrophotometer. C, H, N (combustion), and Cl (titration with Ag^+) analyses were performed at the University of Michigan microanalysis labs. Elemental analysis of metals and sulfur were performed by Electron Microprobe. Scanning electron microscopy (SEM) was performed on a Hitachi S-570, while transmission electron microscopy (TEM) and electron diffraction patterns were measured on a Philips CM12, all part of the Electron Microscopy Analysis Laboratory at the University of Michigan. Samples were prepared for TEM by suspending the powder in acetone and dip-coating a lacy carbon grid. A very thin layer of gold was sputtered onto some samples to give an internal reference for lattice spacings.

Magnetic susceptibility measurements were taken on a Quantum Designs MPMS SQUID magnetometer with an applied field of 1000 G. Magnetizations were measured through a temperature range of 10−300 K. The samples were contained in calibrated gelatin capsules held in the center of a soda straw fixed to the end of the sample rod. The magnetization values of the instrument were calibrated against a standard palladium sample supplied by Quantum Design.

Powder X-ray diffraction patterns of all samples were collected using Cu Kα radiation on various instruments: the patterns for air stable materials were taken on a Philips diffractometer or a Rigaku $\theta-\theta$ diffractometer, and variable temperature experiments were performed on a Scintag x1 with a high temperature/high vacuum chamber attachment. The Li_xMoS_2 was affixed to glass slides via double-sided tape in an inert atmosphere box and then sealed under more tape and transferred to the diffractometer (Rigaku Rotaflex) in vials. No oxidation damage was observed for the tape-covered sample, although it was exposed to air during the scan (25 min). Silicon powder (National Bureau of Standards) was added to the samples as a standard for XRD spacing. Patterns were analyzed on Rigaku software.

X-ray Absorption Spectra. Samples were ground to a fine powder and diluted with BN in a mortar to form a homogeneous mixture which was then packed into a 0.5 mm thick aluminum cell (for first row transition metals) or a 1.0 mm cell with Kapton tape windows. The cells were held in an aluminum holder which was placed in the sample chamber of an Oxford CF-1204 liquid helium flow cryostat. The Li_xMoS_2 sample was prepared as described above in a nitrogen atmosphere box.

X-ray absorption spectra were measured at 10 K at the Stanford Synchrotron Radiation Laboratory (SSRL) on beam line II-3, with synchrotron energies of 3.0 GeV and a stored current of 100 mA. A Si(220) double-crystal monochromator was used and was detuned 50% for harmonic rejection. The monochromator was calibrated using the appropriate metal foil as an internal standard, with the first inflection point of the foil defined as 7112.0 eV (Fe), 7709.0 eV (Co), or 20000.0 eV (Mo). All spectra were collected in transmission mode, using ionization chambers filled with nitrogen (Fe, Co) or argon (Mo).

The Fe spectra were recorded from 6800 to 8000 eV with a step size of 5 eV in the preedge (6800−7050 eV), 0.25 eV in the edge (7050−7140), and 0.05 $Å^{-1}$ in the EXAFS region (7140−8000 eV). Integration times were 1 s in the preedge and edge regions and varied from 1 to 15 s at $k = 15$ $Å^{-1}$ for a total scan time of ca. 35 min. For the Co samples, spectra were recorded from 7500 to 8500 eV with a step size of 5 eV in the preedge (7500−7700 eV), 0.25 eV in the edge (7700−7740), and 0.05 $Å^{-1}$ in the EXAFS region (7740−8500 eV). Integration times were as described above. Mo spectra were recorded over various regions, all starting at 19 700 eV, with k_{max} ranging from 17 to 24 $Å^{-1}$ (21 200 to 22 300 eV) depending on data quality. The step size was 5 eV in the preedge (19700−19950 eV), 0.25 eV in the edge (19950−20040), and 0.05 $Å^{-1}$ in the EXAFS region (20 040−22 300 eV). One sample, MoS_2,

(20) Tsai, H.-L.; Heising, J.; Schindler, J. L.; Kannewurf, C. R.; Kanatzidis, M. G. *Chem. Mater.* **1997**, *9*, 879.
(21) Joensen, P.; Crozier, E. D.; Alberding, N.; Frindt, R. F. *J. Phys. C: Solid State Phys.* **1987**, *20*, 4043.
(22) Yang, D.; Frindt, R. F. *Mol. Cryst. Liq. Cryst.* **1994**, *244*, 355.
(23) Yang, D.; Sandoval, S. J.; Divigalpitiya, W. M. R.; Irwin, J. C.; Frindt, R. F. *Phys. Rev. B* **1991**, *43*, 12053.
(24) Sandoval, S. J.; Yang, D.; Frindt, R. F.; Irwin, J. C. *Phys. Rev. B* **1991**, *44*, 3955.
(25) Qin, X. R.; Yang, D.; Frindt, R. F.; Irwin, J. C. *Ultramicroscopy* **1992**, *42−44*, 630.
(26) Qin, X. R.; Yang, D.; Frindt, R. F.; Irwin, J. C. *Phys. Rev. B* **1991**, *44*, 3490.
(27) Schumacher, A.; Scandella, L.; Kruse, N.; Prins, R. *Surf. Sci. Lett.* **1993**, *289*, L595.
(28) Kelty, S. P.; Ruppert, A. F.; Chianelli, R. R.; Ren, J.; Whangbo, M.-H. *J. Am. Chem. Soc.* **1994**, *116*, 7857.
(29) Wypych, F.; Schöllhorn, R. *J. Chem. Soc., Chem. Commun.* **1992**, 1386.
(30) Wypych, F.; Weber, T.; Prins, R. *Surf. Sci.* **1997**, *380*, L474.
(31) Schöllhorn, R., private communication.
(32) Sheats, J.; Kirsch, T. *Synth. Inorg. Met.-Org. Chem.* **1973**, *3*, 59.
(33) King, R. B. *Organometallic Synth.* **1965**, *1*, 70.
(34) Bjerrum, J.; McReynolds, J. P. *Inorg. Synth.* **1946**, *2*, 216.
(35) Joensen, P.; Frindt, R. F.; Morrison, S. R. *Mater. Res. Bul.* **1986**, *21*, 457.

was collected with an interval of 0.025 $Å^{-1}$ in the EXAFS region. Integration times were 1 s in the preedge and edge regions and varied from 1 s to 15 s at $k = 17$ $Å^{-1}$ (or 20 s at $k = 24$ $Å^{-1}$) for a total scan time of ca. 60 min. The beam size was 1 × 12 mm^2. Two or three spectra were collected and averaged for each sample.

Data Analysis. Data analysis was performed according to established methods.[36] Edge data were normalized by fitting the smoothly varying parts of the absorption spectrum both below and above the edge to tabulated X-ray cross-sections, using a single polynomial background and scale factor.[37] The EXAFS data were converted to k space using an initial E_0 value of 7725 eV for Co and 20 025 eV for Mo and were weighted by k^3 in order to compensate for the decreased EXAFS amplitude at high k. For the Co spectra, the EXAFS signal $k^3\chi(k)$ was truncated at 2.0 and 14.0 $Å^{-1}$ and then Fourier transformed. The Mo EXAFS signal $k^3\chi(k)$ was truncated at 2.0 and 17.0 or 24.0 $Å^{-1}$. The data were Fourier filtered to isolate the contributions corresponding to each peak in the Fourier transform.

The best-fit bond lengths, coordination numbers, and Debye−Waller factors were determined from fitting both the unfiltered and Fourier filtered data using theoretical amplitude and phase functions. The theoretical EXAFS parameters were obtained using ab initio calculations (FEFF, version 6.01) which account for multiple scattering interactions.[38−40] The correct scale factor and threshold energy (E_0) for the theoretical parameters were determined by fitting the EXAFS data for crystallographically characterized model complexes of Co and 2H-MoS_2. When fitting unknown compounds, only the bond length and Debye−Waller factor for each shell were allowed to vary while the coordination number was systematically varied in appropriate steps.

Preparation of Exfoliated and Restacked MoS_2 (2). A vial was charged in the drybox with Li_xMoS_2 (**1**) (0.14 g, 0.84 mmol) and taken out. The vial was opened, 10 mL of H_2O was quickly added, and the resulting mixture was sonicated and shaken for 1 h. The basic mixture was neutralized with 0.5 M HNO_3 and then placed in a polypropylene centrifuge tube and ultracentrifuged (13 000 rpm) for 10 min. The brown decantate was removed and the solid washed twice with H_2O, ultracentrifuged, and then dried in vacuo at 70° C for 4.5 h, yielding a metallic gray powder (0.055 g, 0.34 mmol, 41%). Anal. Calcd for MoS_2: Mo, 59.94; S, 40.06. Obsd: Mo, 60.18; S, 38.21.

Preparation of Co_aMoS_2 (3). (a) In the drybox, a 500 mL round-bottom flask was charged with **1** (0.488 g, 2.92 mmol). H_2O (500 mL) was quickly added to the flask, after removal from the drybox, and the resulting black mixture was shaken and sonicated for 0.5 h. The pH of a 0.6 M solution of $Co(NO_3)_2$ in H_2O (100 mL, 58.44 mmol) was raised to approximately 6.6 by addition of 15 drops of 0.5 M KOH. The black suspension of MoS_2 was added dropwise with stirring to this solution. A black, flaky solid quickly formed and was isolated by centrifugation and then washed in acid (0.5 M HNO_3) and H_2O until the decantate was colorless. The black solid was dried in vacuo at room temperature for 8 h, yielding 0.329 g (1.76 mmol, 60.2% yield). Anal. Calcd for $[Co(OH)_2]_{0.27}MoS_2$: Co, 8.59; Mo, 51.81; S, 34.63. Obsd: Co, 8.13; Mo, 49.67; S, 32.67.

(b) In the drybox a 50 mL Schlenk flask was charged with **1** (0.200 g, 1.2 mmol) and removed**.** A 1 M aqueous solution of $Co(NO_3)_2$ (20 mL, 20 mmol), adjusted to pH 6.6 with 1 M KOH, was quickly added to the flask. The mixture was sonicated for 45 min with vigorous shaking, and bubbles were observed, while the pH decreased to 6.3. The suspension was centrifuged, and the solid was washed with 20 mL of 0.5 M HNO_3, centrifuged, washed, and centrifuged three times with water, and dried in vacuo at 60° C. A dark purple powder was recovered. Anal. Calcd for $[Co(OH)_2]_{0.57}MoS_2$: Co, 15.77; Mo, 45.03; S, 30.10. Obsd: Co, 15.44; Mo, 44.25; S, 28.90.

Preparation of Co_cMoS_2 (4). A vial was charged with **1** (0.222 g, 1.3 mmol) in the glovebox and removed. A 0.2 M aqueous solution $[Co(NH_3)_6]Cl_3$ (20 mL, 0.1 mmol), adjusted to pH 12.3 by addition of 0.5 M KOH, was quickly added to the vial. The mixture was shaken and sonicated for 0.5 h and then centrifuged. The red solution was decanted, and the black solid was washed twice with H_2O and then dried in vacuo at 60 °C for 5.5 h. Anal. Calcd for $[Co(OH)_2]_{0.76}MoS_2$: C, 0; H, 0.66; N, 0; Cl, 0; Co, 19.41; Mo, 41.58; S, 27.80. Obsd: C, 0.93; H, 1.32; N, 0.57; Cl, 0; Co, 18.70; Mo, 40.12; S, 25.31.

Preparation of $(Cp_2M)_xMoS_2$ (5a, M = Co; 5b, M = Fe). In a typical procedure, a 500 mL round-bottom flask was charged in the drybox with **1** (0.498 g, 2.98 mmol). Upon removal of the flask from the drybox, 500 mL of H_2O was quickly added and the resulting black mixture sonicated for 0.5 h. To remove any unreacted MoS_2, the mixture was centrifuged at 2500 rpm for 5 min, and the black suspension was decanted off a black sludge. To this suspension was added with stirring 100 mL of 0.01 M aqueous Cp_2FeCl (pH 0.69). A black, flaky precipitate formed immediately and was separated from the blue solution by centrifuging. It was then washed with 100 mL of 0.5 M HNO_3 and then 200 mL of H_2O and dried in vacuo at 60 °C for 13 h, yielding a black powder (0.133 g, 0.69 mmol, 23%). Anal. Calcd for $(Cp_2Fe)_{0.15}MoS_2$: C, 9.58; H, 0.80; Fe, 4.46; Mo, 51.04; S, 34.12. Obsd: C, 10.51; H, 1.06; Fe, 4.25; Mo, 47.71; S, 25.86. Anal. Calcd for $(Cp_2Co)_{0.14}MoS_2$: C, 9.01; H, 0.76; Co, 4.42; Mo, 51.43; S, 34.38. Obsd: C, 11.65; H, 0.99; Co, 4.25; Mo, 48.99; S, 32.16.

Preparation of TEM Sample of 4. An epoxy pellet was prepared by thoroughly mixing in a 4:1 ratio Lo-Visc Epoxy Resin with Lo-Visc Epoxy Hardener (Mager Scientific) and then halfway filling a 1 in. diameter sample holder (Struers). The resin was hardened by heating it overnight on a hot plate. A suspension of approximately 0.1 g of **4** in acetone was layered on the epoxy and allowed to dry. Another layer of epoxy was made on top of the sample layer. After hardening, a thin section (<1 mm) was cut out with a diamond-tipped, water-cooled saw, such that the thin section was perpendicular to the sample layer. The thin section was mounted onto an aluminum washer with epoxy resin and milled with an argon ion gun.

Results and Discussion

Synthesis of MoS_2 Intercalation Compounds. The synthetic technique used here for the intercalation of MoS_2 has been discussed previously.[6] To summarize, 2H-type (undistorted) MoS_2 was intercalated with Li, forming Li_xMoS_2 (**1**). When **1** was allowed to react with H_2O (in a sonication bath to increase the rate of reaction), the Li^+ cations were hydrated and the negatively charged MoS_2 layers reduced H_2O to H_2 and OH^- (Scheme 1). The microbubbles of H_2 gas produced between the MoS_2 sheets forced them apart (exfoliation) to give an aqueous suspension of partially negatively charged, single layers of MoS_2. Upon addition of H^+, the layers are discharged, presumably with the formation of H_2, and the single layers were flocculated to give "restacked" MoS_2 (**2**). Addition of metal cations to the suspension of single-layer MoS_2 gave the intercalation compounds **3**−**5**.

Structure of 1T-MoS_2. The intercalation of 2H-MoS_2 by Li is known to induce a structural change.[19,41]

(36) Teo, B. K. *EXAFS: Basic Priciples and Data Analysis*; Springer-Verlag: Berlin, 1986.
(37) Waldo, G. S. Ph.D. Thesis, The University of Michigan, 1991.
(38) Rehr, J. J.; Mustre de Leon, J.; Zabinsky, S. I.; Albers, R. C. *J. Am. Chem. Soc.* **1991**, *113*, 5135.
(39) Mustre de Leon, J.; Rehr, J. J.; Zabinsky, S. I. *Phys. Rev. B* **1991**, *44*, 4146.
(40) O'Day, P. A.; Rehr, J. J.; Zabinsky, S. I.; Brown, G. E., Jr. *J. Am. Chem. Soc.* **1994**, *116*, 2938.
(41) Py, M. A.; Hearing, R. R. *Can. J. Phys.* **1983**, *61*, 76.

Table 1. Fitting Parameters[a] for Mo EXAFS of Intercalation Compounds

	Mo−S			Mo−Mo			Mo···Mo			Mo···Mo			
sample	CN	*R*	σ^2	CN	*R*	σ^2	CN	*R*	σ^2	CN	*R*	σ^2	*F*
1	6	2.44	10.4	3	2.94	8.3				3	3.65	11.0	0.057
2	4.28	2.42	4.1	0.49	2.77		1.14	3.17		0.29	3.77		0.045
3a	4.16	2.42	3.8	0.56	2.77		1.32	3.17		0.40	3.79		0.025
4	3.56	2.42	4.6	0.70	2.77		0.66	3.15		0.51	3.79		0.024
5a	4.46	2.42	4.0	0.91	2.77		1.01	3.16		0.65	3.80		0.018
5b	4.49	2.42	4.2	0.82	2.76		0.90	3.16		0.60	3.78		0.045
2H-MoS_2	6.0	2.42	2.8				6.0	3.16	1.6				0.058

[a] CN is the number of scatterers, *R* is the absorber−scatterer distance in Å, σ^2 is the Debye−Waller factor in Å$^2 \times 10^3$ for each shell (note: σ^2 for each Mo shell in samples **2**−**5** set to 1.6 Å$^2 \times 10^3$, see text). $F = ([\Sigma(\chi_{obs} - \chi_{calc})^2]/[N_{pts} - N_{var}])^{0.5}$, the goodness of fit index. The threshold energy (E_o) for all shells in all fits was 24.0 eV, while the scale factor was set to 1.1.

Scheme 1

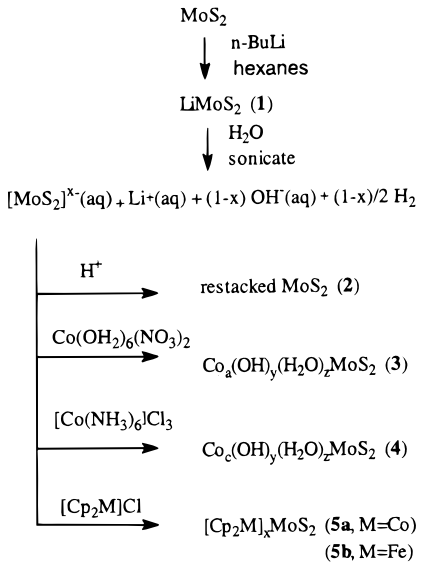

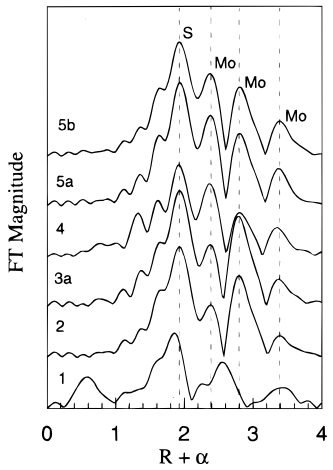

Figure 1. FT of Mo K edge EXAFS for Li_xMoS_2 (**1**), restacked MoS_2 (**2**), $[Co(OH)_2]_{0.27}MoS_2$ (**3a**), $[Co(OH)_2]_{0.76}MoS_2$ (**4**), $(Cp_2Co)_{0.14}MoS_2$ (**5a**), and $(Cp_2Fe)_{0.15}MoS_2$ (**5b**).

In 2H-MoS_2, the sulfur atoms are in hexagonal close-packed sheets. Planes of Mo atoms are sandwiched between alternating sulfur layers such that each Mo is coordinated to six S atoms in a trigonal prismatic geometry. In the unit cell, there are two such sandwiches, with an *aBa bAb* stacking pattern along the *c* lattice direction (lowercase letters correspond to the sulfur planes, while uppercase symbols denote the position of the Mo planes).[42] The region between the sandwiches (the *a* and *b* sulfur planes) is held together by weak van der Waals forces. Upon intercalation, the Li atoms donate electrons to the d-band of the MoS_2 host and Li^+ cations migrate into the interlamellar spacing. The reduced MoS_2 layers transform into the 1T-MoS_2 structure type with octahedrally coordinated Mo atoms and an *aBc aBc* stacking pattern in the *c* lattice direction, such that there is one sandwich layer per unit cell. In addition, electron diffraction studies determined a 2 × 2 superlattice formation in the *a*,*b* lattice directions.

Here is presented the first EXAFS study for Li-intercalated MoS_2 (**1**) that shows the effects of the structural transformation described above (Table 1, Figure 1). The Mo K edge EXAFS were fit to three scattering shells. The first corresponded to six S atoms 2.44 Å from the absorbing Mo atom. The two outer shells were fit with Mo atoms at 2.94 and 3.65 Å. These data indicated that there was an intralayer distortion of the Mo atoms. The shifting of the Mo atoms should result in a distorted octahedral coordination, with a range of Mo−S distances. Evidence for this distortion was found by comparing the disorder (Debye−Waller factor) of the first shell in the Mo EXAFS with that of pristine 2H-MoS_2 ($\sigma^2 = 10.4$ vs 2.8×10^{-3} Å^2). Although the Mo−S distance did not shift significantly from that of 2H-MoS_2 (2.42 Å), the larger σ value indicated that a range of Mo−S distances was present, but EXAFS only resolved the average (2.44 Å) local structure of the bulk sample.

In the previously reported electron diffraction study of Li_xMoS_2, it was assumed that the positions of the Li cations were causing the superstructure.[19] If $x = 0.75$, then three of every four octahedral sites in the interlamellar spacing would be occupied by Li^+, while if $x = 1.25$, then every octahedral site would be filled and one tetrahedral site would also be filled for every four MoS_2 units. However, it seems unlikely that there would be such ordering of the Li cations in the interlamellar spacing. The Mo K edge EXAFS data show that the superstructure is due to the intralayer distortion of the Mo atoms due to the formation of Mo−Mo bonds in the reduced structure.

Upon exfoliation of **1** and flocculation to form restacked MoS_2 (**2**) and intercalated MoS_2 (**3**−**5**), the 1T-MoS_2 structure was partially maintained. The X-ray powder pattern for **2** had a single, weak, broad diffraction peak corresponding to the 002 reflection of 2H-MoS_2. As very limited structural information could be obtained by this technique, the X-ray absorption spectroscopy of the

(42) Liang, W. Y. In *Intercalation in Layered Materials*; Plenum Press: New York, 1986; Vol. 148; p 31.

restacked material was investigated. The Mo K edge EXAFS data were fit to four nearest neighbor scattering shells (Table 1, Figure 1). The first was an Mo−S bond at 2.42 Å, which was similar to the Mo−S distance in **1** and exactly the Mo−S distance in 2H-MoS_2.[43] Unlike in **1**, however, there were three shells corresponding to Mo scatterers at distances of 2.77, 3.16, and 3.79 Å. As the middle distance was exactly the Mo−Mo distance found in pristine 2H-MoS_2, a model involving a heterogeneous mixture of 1T-MoS_2 and 2H-MoS_2 structures was proposed to account for the three different Mo−Mo distances present in the samples.[44]

The presence of a mixture of MoS_2 structures in the restacked samples (**2**−**5**) was verified by comparing the varying numbers of Mo atoms in the three scattering shells. The coordination number (CN) and the Debye−Waller factor (σ) are correlated in the fits of EXAFS data. Therefore, σ^2 was held constant at the value calculated for the first Mo−Mo scatterer shell in pristine 2H-MoS_2 (1.6×10^{-3} Å^2) for the fits presented in Table 1. Hence, the coordination numbers can be compared between samples. The ratios of coordination numbers between the first and second Mo shells (2.77 and 3.16 Å) ranged from 0.4 to 1.0 in different samples, while the ratios of coordination numbers between the first and third Mo shells (2.77 and 3.79 Å) were identical for all the samples within the precision of the calculations (1.4 ± 0.2). These ratios support a model in which the samples consist of a heterogeneous mixture of two phases, one with two Mo−Mo distances (2.77 and 3.79 Å) and the other with one Mo−Mo distance of 3.16 Å.

The presence of two different phases was further confirmed by variable temperature electron diffraction. Diffraction by planes perpendicular to the [002] zone axis of crystallites of restacked MoS_2 (**2**) showed the presence of a 2 × 2 superlattice (Figure 2). The hexagonal *a*-lattice parameter measured from the superstructure phase (spot **s** in Figure 2, due to −1010) was 6.55 ± 0.05 Å, compared to 3.16 Å for 2H-MoS_2 (spot **m** in Figure 2). Close inspection of the electron diffraction pattern revealed a doubling of the main lattice spots due to the mixture of the 2H-MoS_2 phase and the expanded lattice 1T-MoS_2 phase. The relative intensity of the doubled main lattice spots shifted upon annealing (Figure 3). Initially, at room temperature, the main lattice spot corresponding to (22−40) was dominated by 1T-MoS_2 (d = 5.67 Å). As the temperature was raised to 215 °C, a peak at larger R (d = 5.47 Å) grew in. Finally, at 320 °C, the shorter R peak was almost completely gone. The intensity of the superlattice spots were observed to decrease in a similar manner.

The 1T-MoS_2 phase is known to be metastable and transforms to the thermodynamically stable 2H-MoS_2 at approximately 95 °C, according to a DSC study.[29] Therefore, the metastable, superlattice structure observed in the electron diffraction pattern was due to a 1T-MoS_2-type structural distortion. Combining the *a*,*b*

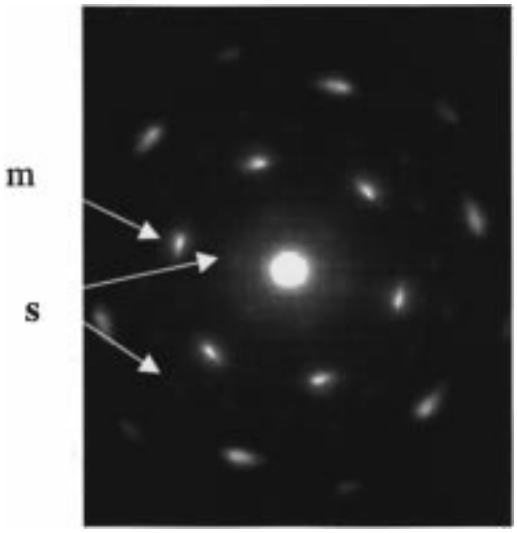

Figure 2. Electron diffraction pattern of **2** along [002] zone axis, where **m** indicates main lattice diffraction spot and **s** indicates superlattice diffraction spot.

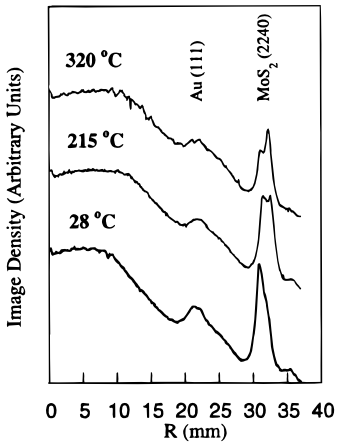

Figure 3. Density profile plots of electron diffraction patterns of **2** at 28 °C, 215 °C, and 320 °C. R is the distance from the undiffracted beam (camera length = 1.6 m, accelerating voltage = 120 kV).

lattice parameters measured from the electron diffraction pattern with the Mo−S and Mo−Mo distances calculated from the Mo K edge EXAFS spectra, a model of the structure of this 1T-MoS_2-type structure is proposed (Figure 4, Table 2). The unit cell, belonging to space group $P3$, is a superstructure of 2H-MoS_2, with $a = b$ = 6.5 Å, c = 6.14 Å, and $\alpha = \beta = 90°$, $\gamma = 120°$. Although the techniques used here cannot distinguish between octahedral and trigonal prismatic coordination around the Mo, the literature consistently favors octahedral coordination for reduced MoS_2. This coordination is distorted, however, as the Mo atoms are shifted approximately 0.5 Å from their positions in 2H-MoS_2 to form linked Mo_3 clusters. The Mo−Mo bond distances in the triangular clusters are 2.76 Å, as are the Mo−Mo bonds linking the clusters.

The structural model proposed above explains the two different Mo−Mo distances and the hexagonal 2 × 2 superlattice. However, a simulated electron diffraction pattern (Cerius^2 from M.S.I.) of the model exhibited diffraction spots for (11−20), (1−100), etc. The observed diffraction pattern has extinctions at (11−20), etc. These extinctions follow no systematic rule and the

(43) Schönfeld, B.; Huang, J. J.; Moss, S. C. *Acta Crystallographie, B* **1983**, *39B*, 404.

(44) Recent theoretical calculations suggest that several structural models for partially reduced MoS_2 layers lie close in energy and that a range of structures may be observed experimentally, depending on the degree of residual negative charge in the layers, their thermal history, etc.: Rousseau, R.; Curtis, M. D.; Canadell, E. Work in progress.

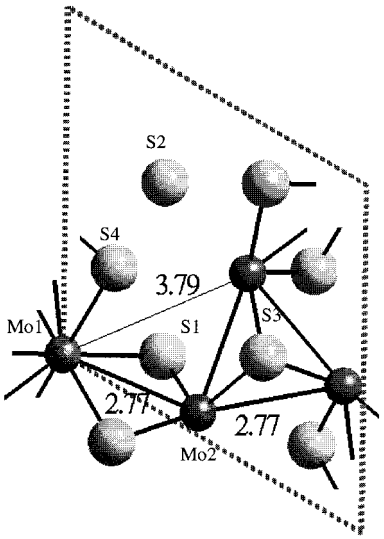

Figure 4. Structural model of 1T-MoS_2 (Mo, dark circles; S, light circles).

Table 2. Atomic Positional Parameters for 1T-MoS_2

atom	*x*	*y*	*z*
Mo1	0.0000	0.0000	0.5000
Mo2	0.9346	0.3881	0.5000
S1	0.3333	0.1667	0.2500
S2	0.3333	0.6667	0.2500
S3	0.6667	0.3333	0.7500
S4	0.1667	0.3333	0.7500

diffraction spots could actually be present but too weak to observe. Indeed, the electron diffraction pattern of restacked WS_2 does exhibit diffraction spots at (11−20).[20]

The structure of the intralayer Mo−Mo distortion presented above was proposed as a possible charge density wave (CDW) distortion for d^3 transition-metal dioxides based upon electronic structure calculations.[45] Band structure and density of states (DOS) calculations have been performed on this proposed structure (Figure 5).[46] Unlike 2H-MoS_2, which contains a large gap at the Fermi level, the Fermi level for 1T-MoS_2 (assuming $[MoS_2]^{-0.25}$) is in the middle of a band. In response to reduction, the structure of MoS_2 distorts to decrease the band gap between the valence and conduction bands. The distortion includes formation of Mo−Mo bonds and a change in coordination from trigonal prismatic to octahedral. On the basis of these calculations, 1T-MoS_2 would be expected to be metallic, as observed.[29] Further calculations are in progress to determine the relative stabilities of several possible structural models for partially reduced MoS_2.[44]

An intriguing structural relationship exists between 1T-MoS_2 and molecular Mo−S clusters. The shorter Mo−Mo distance (2.77 Å) is in the range of the Mo−Mo bond lengths observed in cuboidal clusters with Mo_3S_4 cores (2.73−2.83 Å).[47] In addition, raft-type Mo_6S_8 clusters show the same structural motif of Mo_3 triangles joined by Mo−Mo bonds.[48,49]

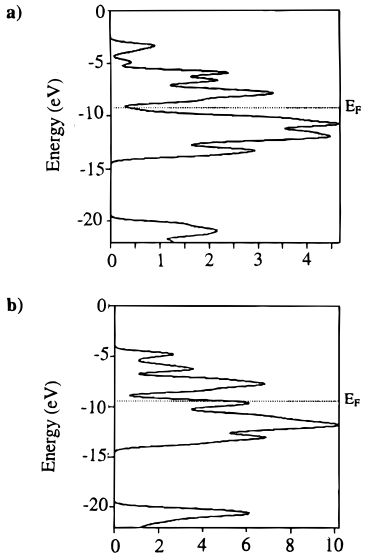

Figure 5. Density of states of (a) 2H-MoS_2 and (b) 1T-MoS_2.

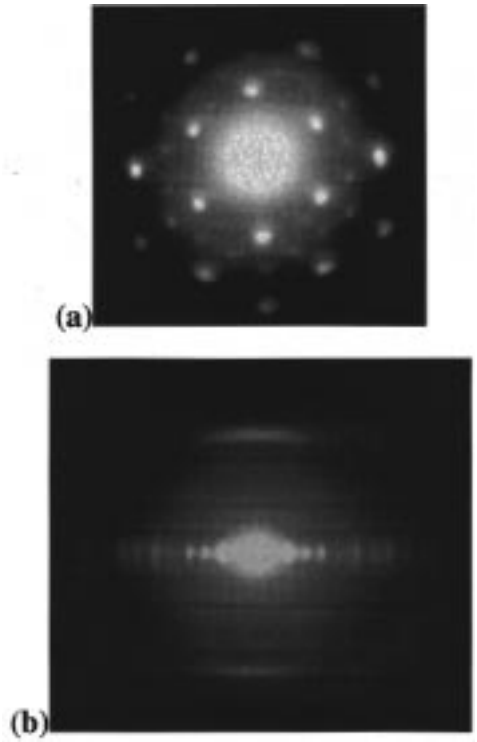

Figure 6. Electron diffraction patterns of **4** along (a) [00*l*] and (b) [*hk*0] zone axes.

Structure of MoS_2 Intercalation Compounds. As discussed above, the Mo K edge EXAFS of the intercalation compounds of MoS_2 (**3**−**5**) were fit by a mixture of 1T-MoS_2 and 2H-MoS_2 phases. The electron diffraction patterns (e.g. for sample **4**, Figure 6a) exhibited the same superstructure observed in the electron diffraction pattern of **2**. Therefore, the same distorted phase of MoS_2 (1T-type) present in restacked MoS_2 was present in the intercalated materials.

The fact that intercalation had occurred upon restacking the MoS_2 in the presence of metal guest was observed by electron diffraction when the sample (**4**) was prepared such that the basal planes of the microcrystallites were parallel to the electron beam (Figure 6b). This orientation afforded diffraction spots due to 00*l*,

(45) Burdett, J. K.; Hughbanks, T. *Inorg. Chem.* **1985**, *24*, 1741.
(46) Landrum, G. *YAeHMOP—Yet Another Extended Hückel Molecular Orbital Package*, Version 1.2; Ithaca, New York, 1995.
(47) Shibahara, T. *Adv. Inorg. Chem.* **1991**, *37*, 143.
(48) Mizutani, J.; Yamada, S.; Imoto, H.; Saito, T. *Inorg. Chem.* **1996**, *35*, 244.
(49) Tsuge, K.; Imoto, H.; Saito, T. *Inorg. Chem.* **1992**, *31*, 4715.

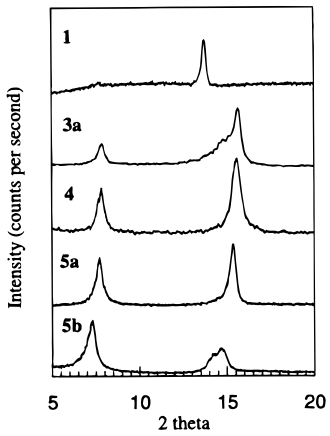

Figure 7. Powder X-ray diffraction patterns of **1**, **3a**, **4**, **5a,** and **5b**.

Table 3. Summary of Data for Powder X-ray Diffraction

compd	d (Å) (hkl)		Δc (Å)[a]
MoS_2	6.14 (002)	$c/2$	0.00
1	6.29 (002)	$c/2$	0.15
3a	11.20 (001)	c'	5.06
4	11.34 (001)	c'	5.20
5a	11.30 (001)	c'	5.16
5b	11.63 (001)	c'	5.49

[a] Δc = lattice expansion as defined in Scheme 2.

Scheme 2

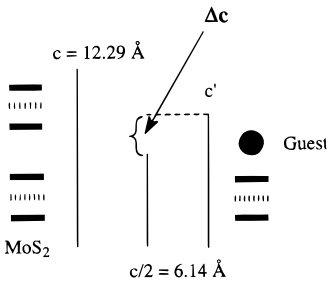

as c^* was perpendicular to the electron beam. Indexing these spots yielded a c lattice parameter (11.6 ± 0.2 Å) which indicated a lattice expansion of 5.4 Å, compared to 2H-MoS_2. X-ray diffraction of all the intercalated samples (**3**−**5**) were also consistent with a lattice expansion in the c direction, when compared to 2H-MoS_2 (Figure 7). The powder patterns showed only 001 and 002 diffraction peaks at $2\theta = 7.7°$ and 15.4°, which were quite distinct from the 002 diffraction peak of 2H-MoS_2 at $2\theta = 14.4°$. Table 3 summarizes the d spacings corresponding to the diffraction patterns presented in Figure 7, and Scheme 2 demonstrates the relation between the c lattice parameters of 2H-MoS_2 and intercalated MoS_2. As the layer thickness of 1T-MoS_2 is almost identical to a single layer of 2H-MoS_2 ($c \approx 6.14$ Å $= d_{002}$ for 2H-MoS_2) the c lattice parameters of the intercalates represent an interlayer expansion (Δc) of approximately 5.1 Å, commensurate with the intercalation of one layer of the guest species.

Scanning electron microscopy (SEM) of all the samples indicated that the material was composed of flat particles, about 1 μm thick and 3−10 μm in diameter. These formed larger agglomerates, ranging from 100 μm to almost 1 mm, depending on the preparation conditions. In the same experiment, energy-dispersive X-ray (EDX) spectra were taken to obtain qualitative composition information, which indicated that the Co (or Fe) and Mo were distributed homogeneously in all the samples described herein.

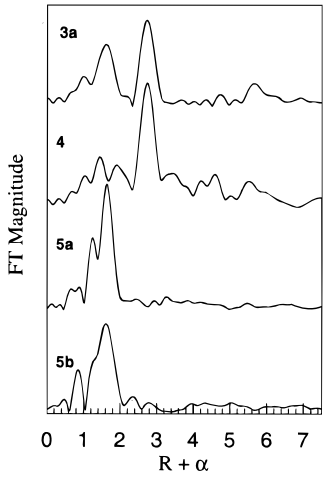

Figure 8. FT of Co K edge EXAFS for **3a**, **4**, and **5a** and FT of Fe K edge EXAFS for **5b**.

Table 4. Fitting Parameters[a] of Co Edge EXAFS for Co^{+2} and Co^{+3} Intercalation Compounds

	Co−O			Co			Co				
sample	CN	R	σ^2	CN	R	σ^2	CN	R	σ^2	sf	F
3a	6	2.07	6.5	6	3.13	5.8	6	6.28	7.6	0.7	0.019
4	6	2.07	10.4	6	3.11	2.9				0.7	0.28
$Co(OH)_2$	6	2.09	4.7	6	3.17	2.8	6	6.35	3.3	0.9	0.11

[a] CN is the number of scatterers, R is the absorber−scatterer distance in Å, σ^2 is the Debye−Waller factor in Å$^2 \times 10^3$ for each shell. $F = ([\Sigma(\chi_{obs} - \chi_{calc})^2]/[N_{pts} - N_{var}])^{0.5}$, the goodness of fit index. sf is the scale factor for each shell. The threshold energy (E_o) for all shells in all the fits was 5.5 eV.

No nonintercalated 2H-MoS_2 was detected by X-ray diffraction or electron diffraction. Yet undistorted MoS_2 layers were present, as demonstrated by the Mo−Mo distance of 3.16 Å observed in the Mo K edge EXAFS. Therefore the intercalated compounds consisted of alternating layers of guest monolayers and MoS_2 sheets having both distorted (1T-type) and undistorted (2H-type) structures.

The natures of the intercalated guest species were determined by examining the local structure about the intercalated metal atoms with EXAFS. When $[Co(OH_2)_6](NO_3)_2$ was the precursor complex, the Co K edge EXAFS of the resulting intercalation compound, **3a,** was fit with three nearest neighbor scatterer shells (Figure 8, Table 4). The first corresponded to six O atoms at 2.07 Å, while the other two shells were fit with Co scatterers of six atoms each, at 3.13 and 6.28 Å from the absorbing Co. These distances and coordination numbers were the same as those found in $Co(OH)_2$, a layered compound with the CdI_2 structure.[50] Recent Co EXAFS studies of Co(II)-intercalated MoS_2 agree with the assignment of the intercalated phase as $Co(OH)_2$.[51,52]

(50) Lotmar, W.; Feitknecht, W. *Z. Kristallogr., Kristallogr., Kristallogr., Kristallogr.* **1936**, *93*, 368.

(51) Valeev, E. F.; Zubavitchus, Y. V.; Slovokhotov, Y. L.; Golub, A. S.; Protzenko, G. A.; Novikov, Y. N. *Physica B* **1995**, *298 & 209*, 569.

(52) Zubavichus, Y. V.; Golub, A. S.; Novikov, Y. N.; Slovokhotov, Y. L.; Nesmeyanov, A. N.; Schilling, P. J.; Tittsworth, R. C. *J. Phys. Fr.* **1997**, *7*, 1057.

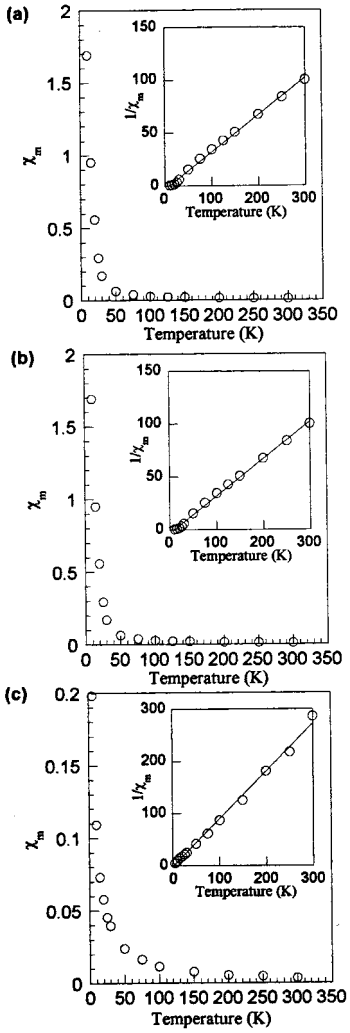

Figure 9. Magnetic susceptibility of (a) **3b**, (b) **4**, and (c) **5b**.

Additional evidence for the $Co(OH)_2$ phase was given by the magnetic susceptibility measurements (Figure 9a). The temperature-dependent behavior (linear $1/\chi$ vs T curve) and room-temperature effective magnetic moment ($4.89\mu_B$ per Co) of **3b** were identical to that expected for octahedrally coordinated Co^{2+} (high spin d^7 with a large spin−orbit coupling). A very recent study found that the magnetic susceptibility of Co(II)-intercalated MoS_2 compared favorably to that of Co-$(OH)_2$, in agreement with the results presented here.[53]

Surprisingly, very similar EXAFS and magnetic results to those for **3** were obtained when $[Co(NH_3)_6]$-Cl_3 was the precursor complex (**4**). The Co K edge EXAFS were fit with two nearest neighbor scatterer shells. The first shell corresponded to six O atoms at 2.07 Å, while the second shell was fit with six Co atoms at 3.11 Å. Unlike **3a**, a third shell, consisting of Co atoms, was not detected. Another difference was an increase in the Debye−Waller factor of the O shell for **4** as compared with that of **3a** (10.4 vs 6.5×10^{-3} Å^2). Both of these differences indicate an increase in disorder or a decrease in particle size of the $Co(OH)_2$ phase in **4**.

However, the magnetic susceptibility per Co atom of **4** was identical to that of **3b** (Figure 9b). Both had

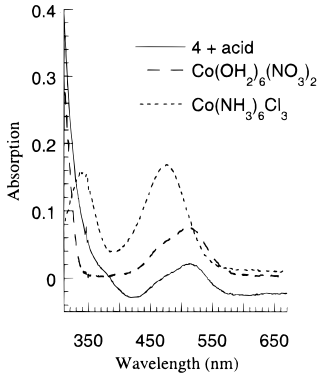

Figure 10. UV−vis spectroscopy of acid extraction of **4**, compared with aqueous solutions of Co complexes.

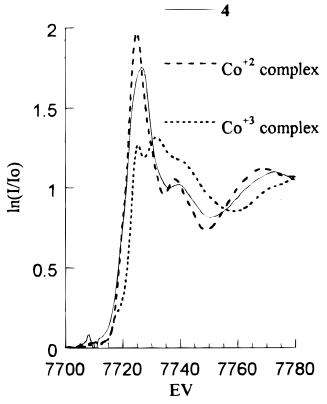

Figure 11. XANES spectrum of Co K edge for **4**, compared with those of Co complexes.

linear $1/\chi$ vs T curves and μ_{eff} of 4.89 μ_B per Co at room temperature. An explanation for the similarity of the magnetic behavior is that the exfoliated MoS_2 had reduced the Co^{3+} complex. This possibility is also suggested by the very low N content as determined by elemental analysis of **3b**. $Co(NH_3)_6^{3+}$ is inert to ligand exchange (low spin d^6), so the absence of NH_3 ligands on the intercalated cobalt ions indicate that the Co(III) was reduced to Co(II) during the intercalation process. Co(II) is labile and would exchange NH_3 for solvent (H_2O) or hydroxide ion very rapidly.[54] In addition, a hydrochloric acid extraction of **4** resulted in a pink solution whose absorption spectrum matched that of $[Co(OH_2)_6]^{2+}$ (Figure 10). Finally, the reduced Co in **4** was observed in the Co K edge XANES spectrum (Figure 11). Comparison with model complexes showed that the Co absorption edge for **4** (at 7720 eV) was the same as that of the Co^{2+} complex $[Co(OH_2)_6](NO_3)_2$ and lower in energy than that of the Co^{3+} complex $[Co(NH_3)_6]Cl_3$ (7723 eV). A higher energy X-ray absorption is expected for a higher oxidation state, and the absorption edge of sample **4** is clearly in the Co^{2+} oxidation state region.

The only possible reducing agent present during the synthesis of **4** is the exfoliated MoS_2 sheets. Hence, these results constitute proof that the single layers of MoS_2 sheets in aqueous suspension are negatively charged. Previously, the partial negative charge of restacked MoS_2 sheets had been inferred from the lack of co-intercalated counterions upon intercalation of

(53) Golub, A. S.; Payen, C.; Protzenko, G. A.; Novikov, Y. N.; Danot, M. *Solid State Commun.* **1997**, *102*, 419.

(54) Shriver, D. F.; Atkins, P. W.; Langford, C. H. *Inorganic Chemistry*; 1st ed.; W. H. Freeman: New York, 1990; p 222.

Table 5. Fitting Parameters[a] of M EXAFS (M = Co in 5a; Fe in 5b) for Organometallic Inclusion Compounds of MoS_2

	M−C					
sample	CN	*R*	σ^2	E_o	sf	*F*
5b	10	2.06	6.2	10	0.9	0.30
5a	10	2.06	2.7	2.2	0.7	0.28
Cp_2CoPF_6	10	2.06	1.5	2.2	0.7	0.60

[a] CN is the number of scatterers, *R* is the absorber−scatterer distance in Å, σ^2 is the Debye−Waller factor in Å^2 × 10^3 for each shell. $F = ([\Sigma(\chi_{obs} - \chi_{calc})^2]/[N_{pts} - N_{var}])^{0.5}$, the goodness of fit index. sf is the scale factor for each shell, and E_o is the threshold energy for each shell.

ammonium cations in MoS_2 ($[NH_4]_{0.25}MoS_2$).[55] The evidence presented above strengthens this conclusion.

The other two precursor complexes, $[Cp_2Co]^+$ and $[Cp_2Fe]^+$ gave different results from the complexes presented above, but similar results to each other. Upon restacking between MoS_2 sheets, they both retained their C ligation, according to Co K edge EXAFS (Figure 8, Table 5). Only one scatterer shell was detected for each sample, which was fit to 10 C atoms. For the $[Cp_2Co]^+$-derived sample (**5a**), the Co−C distance was calculated to be 2.06 Å, which was identical to the value for crystalline $[Cp_2Co]^+$.[56] The $[Cp_2Fe]^+$-intercalated sample (**5b**) had an Fe−C distance of 2.06 Å (versus 2.07 Å in crystalline $[Cp_2Fe]^+$).[57]

The magnetic susceptibility measurements of **5a** and **5b** were consistent with the intercalation of the metallocenium complexes. Sample **5a** had a slightly paramagnetic susceptibility ($\chi = 1 \times 10^{-4}$ emu/mol). As cobaltocenium ion is diamagnetic (low spin d^6), the magnetism of **5a** was due to residual unpaired electrons in the reduced MoS_2 host. The room-temperature magnetic moment of **5b** was $3\mu_B$ per Fe. This value compared favorably with the reported value of 2.62 μ_B for $[Cp_2Fe]PF_6$.[58,59] Values of μ_{eff} near $3\mu_B$ have been observed recently for ferrocenium ion-containing conjugated polymers.[60]

Structural models for the intercalation compounds of MoS_2 with the two types of guests (double hydroxide, metallocenium) are presented in Figure 12. The unit cell consists of one layer of guest and one sheet of MoS_2, having either distorted (1T-type) or undistorted (2H-type) structures. The characterization methods utilized herein do not distinguish between the possible orientations of the metallocenium intercalants, but the *c* axis expansions, 5.2 and 5.6 Å, are comparable to those observed previously for which a perpendicular orientation of the Cp rings with respect to the basal planes was proposed.[61,62] It is interesting to note that the Δc

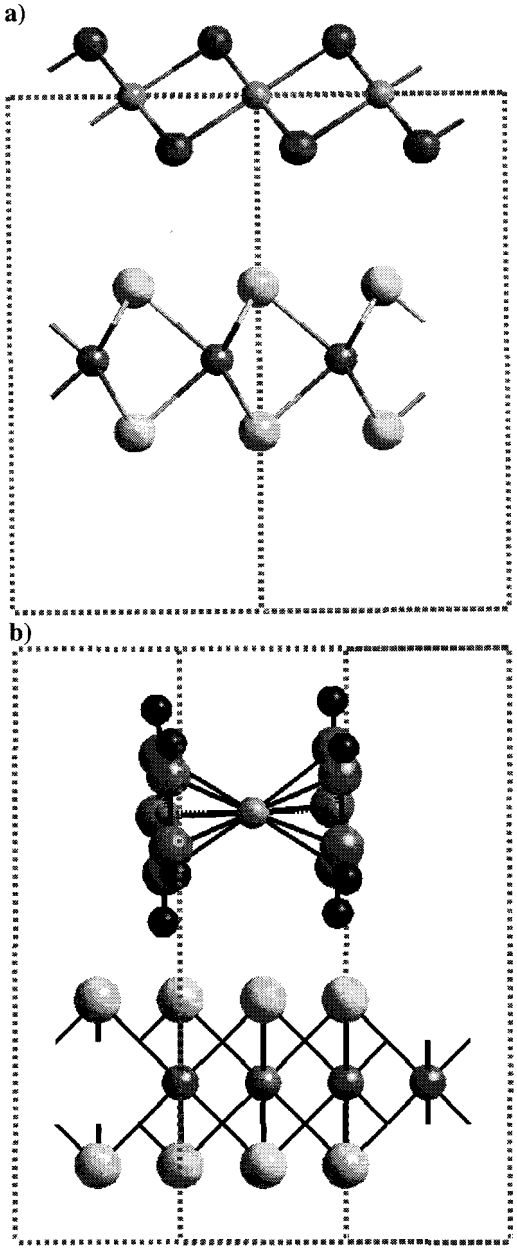

Figure 12. Structural models of (a) **3** and **4** and (b) **5**.

observed here for **5b** is identical to that observed when neutral Cp_2Fe is intercalated into MoS_2.[61,62] However, most of the cobaltocenium intercalation compounds reported in the literature have the Cp rings oriented perpendicular to the basal plane of the host.[63−65] On the other hand, there are a few examples of cobaltocene and cobaltocenium intercalation compounds in which the Cp rings are parallel to the basal planes of the host.[66,67] Future experiments are planned to determine the particular orientation of the metallocenium guests for the MoS_2 intercalation compounds. Elemental analysis revealed no Cl^- counterion present in the metallocenium compounds, so the partially reduced MoS_2

(55) Danot, M.; Mansot, J. L.; Golub, A. S.; Protzenko, G. A.; Fabritchnyi, P. B.; Novikov, Y. N.; Rouxel, J. *Mater. Res. Bul.* **1994**, *29*, 833.
(56) van de Goor, G.; Freyhardt, C. C.; Behrens, P. Z. *Z. Anorg. Allg. Chem.* **1995**, *621*, 311.
(57) Mammano, N. J.; Zalkin, A.; Landers, A.; Rheingold, A. L. *Inorg. Chem.* **1977**, *16*, 297.
(58) Anderson, S. E.; Rai, R. *Chem. Phys.* **1973**, *2*, 216.
(59) Hendrickson, D. N.; Sohn, Y. S.; Gray, H. B. *Inorg. Chem.* **1971**, *10*, 1559.
(60) Southard, G. E.; Curtis, M. D. *Organometallics* **1997**, *16*, 5618−5620.
(61) Divigalpitiya, W. M. R.; Frindt, R. F.; Morrison, S. R. *Science* **1989**, *246*, 369.
(62) Tagaya, H.; Hashimoto, T.; Karasu, M.; Izumi, T.; Chiba, K. *Chem. Lett.* **1991**, 2113.
(63) Wong, H. V.; Evans, J. S. O.; Barlow, S.; Mason, S. J.; O'Hare, D. *Inorg. Chem.* **1994**, *33*, 5515.
(64) Mathey, Y.; Clement, R.; Sourisseau, C.; Lucazeau, G. *Inorg. Chem.* **1980**, *19*, 2773.
(65) Evans, J. S. O.; O'Hare, D. *Chem. Mater.* **1995**, *7*, 1668.
(66) Cleary, D. A.; Francis, A. H. *J. Phys. Chem.* **1985**, *89*, 97.
(67) Clement, R. P.; Davies, W. B.; Ford, K. A.; Green, M. L. H. *Inorg. Chem.* **1978**, *17*, 2754.

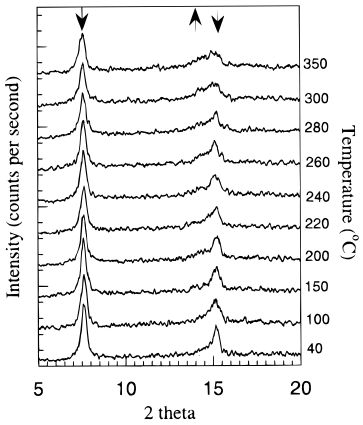

Figure 13. Powder X-ray diffraction patterns of **5a** at various temperatures.

sheets (or possibly interlamellar OH^- ions) must be the counterion. In the $Co(OH)_2$ intercalation compounds, the partial negative charge on the MoS_2 sheets may be offset by the partial substitution of H_2O for OH^- in the guest layers.

Our conclusion that the MoS_2 intercalation compounds consist of mixtures of 1T-type and 2H-type structures in the MoS_2 layers differs from the conclusions reached in a recent EXAFS study.[52] Zubavichus et al. concluded that some intercalates (Mn, Co) have the 2H-MoS_2 structure, while others (Ni, Ru) have a distorted structure. In contrast, each of the intercalation compounds presented here ($Co(OH)_2$, Cp_2Co^+, Cp_2Fe^+) contained both distorted and undistorted MoS_2 layers, though to a differing degree ($0.4 <$ 1T-MoS_2/2H-$MoS_2 < 1.0$). A possible explanation for the conflicting results is that a mixture of MoS_2 phases may be present, yet undetected, in the Zubavichus samples. Another possible explanation is that the Zubavichus samples have been exposed to different thermal histories. The latter explanation is most probable, as the 1T-type distortion of MoS_2 is thermally unstable and exposure to heat or aging in air results in a structural transformation to the 2H-MoS_2 structure. Indeed, Zubavichus et al. present S K and Mo L_{III} edge XANES spectra that indicate the presence of S^{6+} and Mo^{6+} in the Co, Mn, and (to a smaller extent) Ni samples. The oxidized species were due to oxidation damage by long exposure to air, and thus the 2H-MoS_2 phase detected in the Mo K edge EXAFS was most likely due to aged and/or oxidized samples.

Thermal Stability of MoS_2 Intercalates. In the electron microscope, the transition from the 1T- to the 2H-type structures was observed upon annealing restacked MoS_2 (**2**) above 200 °C (Figure 3). In a similar temperature region, an intercalated sample, $(Cp_2Co)_{0.14}MoS_2$ (**5a**), underwent a phase transition to 2H-MoS_2. The variable temperature powder X-ray diffraction patterns are presented in Figure 13. As the temperature was increased to 350 °C, the 001 and 002 diffraction peaks of **5a** decreased in intensity while the 002 diffraction peak for 2H-MoS_2 grew in. Similar structural changes have been observed for the $Co(OH)_2$-intercalated MoS_2 compounds.[11] These changes in the diffraction pattern with temperature indicate that the intercalation compounds are thermally unstable. The instability may be related to the metastability of the 1T-MoS_2 phase. Upon heating (or, more slowly, aging in air), the 1T-MoS_2 phase transforms to the more stable 2H-MoS_2, and simultaneously the guest species are reduced and de-intercalated.

The thermal instability of 1T-MoS_2 may explain the conflicting structural models presented in the literature for restacked MoS_2. Depending upon the sample's thermal history and age, different phases may be present. Therefore, care must be taken when applying different techniques to a sample to ensure that the same phase is being characterized. However, the different experimental conditions necessary for various techniques (e.g. EXAFS, XRD, STM, and AFM) make this a difficult task.

Conclusions

The structure of 2H-MoS_2 distorts upon intercalation with Li such that the Mo atoms became octahedrally coordinated and their positions are shifted to form triangular clusters linked with Mo−Mo bonds. The structural model of 1T-MoS_2 proposed herein is consistent with the EXAFS, XRD, and electron diffraction results. The structural motif (linked Mo_3 clusters) is similar to that found in molecular Mo−S clusters. The superstructure observed in previous literature reports is due to the distortion of the Mo atom positions, rather than to the positions of the Li atoms. The distorted MoS_2 structure (1T-MoS_2) is partially maintained upon exfoliation and restacking. The Mo atoms remain shifted with respect to their positions in 2H-MoS_2 to form trigonal clusters, linked by Mo−Mo bonds. The restacked material consists of a heterogeneous mixture of 1T-type and 2H-type MoS_2 structures.

When the MoS_2 is restacked around guest species, some of the 1T-type distorted MoS_2 remains in the intercalation compound. Formation of intercalation compounds from either Co^{2+}(aqueous) or $Co(NH_3)_6^{3+}$ resulted in a layer of $Co(OH)_2$ alternating with layers of MoS_2 (distorted and undistorted). The reduction of Co^{3+} to Co^{2+} by aqueous suspensions of single MoS_2 layers indicates that the exfoliated MoS_2 sheets are partially negatively charged. Intercalation of $[Cp_2Co]^+$ and $[Cp_2Fe]^+$ into MoS_2 produced a material with alternating layers of metallocenium guest ions and partially negatively charged MoS_2 layers (both 1T- and 2H-type structures).

The distorted MoS_2 phase (intercalated or un-intercalated) is thermally unstable and transforms to 2H-MoS_2 over time or (more quickly) upon heating. Therefore, any characterization of this material must take into account the thermal history of each sample. The conflicting results presented in the literature may be due to differences in sample handling. In addition, the thermal instability of the intercalates limits their applicability (e.g. for hydrodesulfurization catalysts).[18]

Acknowledgment. This work was supported by the National Science Foundation under grant CHE-9523056. We thank Professor Stephen Lee for helpful conversations and the use of his Silicon Graphics workstation and Cerius^2 software for calculation of the ED patterns, DOS, etc. K.E.D. is grateful to the Department of Chemistry for a Margaret and Henry Sokol Fellowship and the College of Literature, Sciences and Arts for a Regent's Fellowship.

CM980034U